SIAM J. IMAGING SCIENCES
Vol. xx, pp. x

Variational Approach for Restoring Blurred Images with Cauchy Noise

Federica Sciacchitano[†], Yiqiu Dong[†], and Tieyong Zeng[‡]

Abstract. The restoration of images degraded by blurring and noise is one of the most important tasks in image processing. In this paper, based on the total variation (TV) we propose a new variational method for recovering images degraded by Cauchy noise and blurring. In order to obtain a strictly convex model, we add a quadratic penalty term, which guarantees the uniqueness of the solution. Due to the strict convexity of our model, the primal dual algorithm is employed to solve our minimization problem. Experimental results show the effectiveness of the proposed method for deblurring and denoising simultaneously images corrupted by Cauchy noise. Comparison with other existing and well known methods is provided as well.

Key words. Cauchy noise, image deblurring, image denoising, primal dual algorithm, total variation regularization, variational model.

AMS subject classifications. 68U10, 94A08, 49J40, 52A41, 65K10, 90C47, 35B45,

1. Introduction.

Image deblurring and image denoising are fundamental problems in the applied mathematics community, see for instance [4, 5]. Most of the literature deals with the restoration of images corrupted by additive Gaussian noise [10, 19, 46, 51]. Unfortunately, in many engineering applications the noise has a very impulsive character and thus it cannot be modeled by this kind of noise. The most common example of impulsive noise is given by the impulse noise [13, 38, 39], which can be caused, for instance, by analogue-to-digital converter errors, by malfunctioning pixel elements in the camera sensors and so on. Another impulsive degradation is given by Cauchy noise, which appears in atmospheric and underwater acoustic noises, radar and sonar applications, air turbulence, wireless communication system, biomedical images, synthetic aperture radar (SAR) images, for an overview we refer the reader to [31, 33, 34, 42, 43, 44].

Mathematically speaking, the degraded image f in presence of blurring and Cauchy noise is given by $f = Ku + v$, where u is the original image defined on the image domain $\Omega \subset \mathbb{R}^2$, K is the blurring operator and v is some Cauchy noise. A random variable V follows the Cauchy distribution, if it has density

$$g(v) = \frac{1}{\pi} \frac{\gamma}{\gamma^2 + (v - \delta)^2}, \tag{1.1}$$

where $\gamma > 0$ is the scale parameter and $\delta \in \mathbb{R}$ is called localization parameter.

Recently, several approaches deal with Cauchy noise, for instance Chang *et al.* [12] used recursive Markov random field models for reconstructing images with Cauchy noise. Achim and Kuruoğlu [1] proposed a method for denoising a image degraded by Cauchy noise in the complex wavelet domain. Wan *et al.* [49] studied a segmentation technique for noisy colour

[†]Department of Applied Mathematics and Computer Science, Technical University of Denmark, Kgs. Lyngby, Denmark (feds@dtu.dk, yido@dtu.dk).

[‡]Department of Mathematics, Hong Kong Baptist University, Kowloon Tong, Hong Kong (zeng@hkbu.edu.hk).

images corrupted by Cauchy noise. As far as we know, in the literature, none has never studied a variational model for removing Cauchy noise, thus, our contribution is to propose a variational model for deblurring and denoising degraded images with Cauchy noise.

One of the most famous variational model is the ROF model. This approach was introduced in 1992 by Rudin, Osher, and Fatemi and it is defined as follows

$$\inf_u J(u) + \frac{\lambda}{2}\int_\Omega (f-u)^2 \mathrm{d}x, \tag{1.2}$$

where $J(u) = \int_\Omega |Du|$ is the total variation (TV) regularization term, the last term is the data fidelity term and $\lambda > 0$ is the regularization parameter, which represents the trade-off between a good fit of f and a smoothness due to the TV regularization term. Due to its capability of preserving sharp edges, it is a very successful and popular algorithm for denoising image corrupted by additive Gaussian noise.

Overall the years, many variational models based on TV have been introduced for removing other noises, such as multiplicative noise [3, 45], impulse noise [16, 18, 39], Poisson noise [36], etc. In our work, inspired by the above studies, we introduce a variational model, based on total variation as regularization term, for denoising and deblurring images with blur and Cauchy noise. In particular, we propose the following problem for removing Cauchy noise,

$$\inf_u J(u) + \frac{\lambda}{2}\int_\Omega \log\Big(\gamma^2 + (u-f)^2\Big)\mathrm{d}x, \tag{1.3}$$

where $\gamma > 0$ is the scale parameter, see (1.1). As one can see, we keep the same regularization term as in the ROF model, but we adapt the data fidelity term to the Cauchy noise, introducing one that is suitable for such kind of noise. We emphasize that TV regularization is very useful tool for preserving edges, but is not so good for texture recovery, thus, clearly, the proposed model can be extended to other modern regularization terms such as nonlocal TV [21], high order TV [50], dictionary learning [19, 28], or tight-frame approach [8].

Unfortunately, since the data fidelity term is not convex, the uniqueness of the solution in (1.3) is not guaranteed. Hence, to overcome this problem we use a quadratic penalty function technique, in particular, we introduce the following convex minimization problem

$$\inf_u J(u) + \frac{\lambda}{2}\left(\int_\Omega \log\Big(\gamma^2 + (u-f)^2\Big)\mathrm{d}x + \mu\|u-u_0\|_2^2\right), \tag{1.4}$$

where u_0 is the image obtained applying the median filter [5] to the noisy image. We employ the median filter in the quadratic penalty term, since it has been shown that it works well for removing impulse noise, [13], and the Cauchy degradation has some similarities with the impulse degradation.

Easily, we can also generalize our model for restoring a blurred image corrupted by Cauchy noise. Given a linear blurring operator K, we consider the following convex model for deblurring and denoising simultaneously

$$\inf_u J(u) + \frac{\lambda}{2}\left(\int_\Omega \log\Big(\gamma^2 + (Ku-f)^2\Big)\mathrm{d}x + \mu\|Ku-u_0\|_2^2\right). \tag{1.5}$$

Due to the strict convexity of the minimization problem, the minimization problem in (1.5) is solved using the primal dual algorithm proposed by Chambolle and Pock in [11].

Numerical results show the potentiality and the effectiveness of the proposed method for restoring blurred images degraded by Cauchy noise. Furthermore, we compare the reconstructed images obtained by our method with the ones given by the ROF model [46], the median filter [20] and the L^1-TV model [39].

The rest of the paper is organized as follows. In Section 2, we describe the alpha-stable distribution, focusing on the Cauchy distribution. Using the MAP estimator, in Section 3 we derive our model for deblurring and denoising simultaneously an image and we analyze some theoretical properties of this model. Adding a quadratic penalty term, which depends on the median filter, in Section 4, we propose a convex model to restore blurred and degraded image by Cauchy noise and we prove the existence and uniqueness of the solution. In Section 5, using the primal dual algorithm, we show some numerical results and we compare them with the reconstructions obtained with other existing approaches. Finally, in Section 6, we draw some conclusions.

2. Cauchy noise modeling.

Many studies in image and signal processing rely on the fundamental assumption that the noise follows a Gaussian distribution. This hypothesis is justified due to the existence of the Central Limit Theorem, see [26]. But, unfortunately, most of the real world problems cannot be modeled by Gaussian distribution, since the noise is much more impulsive than the one that is modeled by additive Gaussian noise. Examples of these applications can be found in the radar and sonar applications, where there are atmospheric and underwater acoustic noises, in biomedical images, in SAR images and so on. These types of noise follow the so called alpha-stable distributions [40, 41, 47].

The alpha-stable distributions were introduced in 1925 by the French mathematician Paul Lévy. The name stable is due to the fact that they are closed under additions, i.e. the sum of two alpha-stable random variables is still a alpha-stable random variable. One of the main advantage of this distribution is that the alpha-stable random variables obey to the Generalized Central Limit Theorem. But, there is also a very important disadvantage, this class has not a close formula for densities and distribution functions (apart from Gaussian, Cauchy and Lévy distributions). The easiest and most common way to define these distributions is through the characteristic function or Fourier transform, see [47].

Generally speaking, an alpha-stable distribution is characterized by four parameters: an index of stability $\alpha \in (0, 2]$, a skewness parameter $\beta \in [-1, 1]$, a scale parameter $\gamma > 0$ and a location parameter $\delta \in \mathbb{R}$. When $\alpha \in (1, 2]$, the location parameter δ corresponds to the mean of the distribution, otherwise δ corresponds to its median. The scale parameter determines the spread of the distribution around δ and it plays a similar rule as the variance in the Gaussian distribution. If $\gamma = 1$ and $\delta = 0$ we say that the distribution is standardized, furthermore if $\beta = 0$ the distribution is symmetric around zero, in this case we call it symmetric alpha-stable distributions. From now on we will focus only on symmetric alpha-stable distributions.

The distributions of this class are all bell-shaped, with increasing density on the left and decreasing on the right. The heaviness of the distribution tails is controlled by the parameter α, i.e., the tails grow thicker as alpha becomes smaller.

In Figure 1, we show the PDFs of symmetric alpha-stable distributions with different

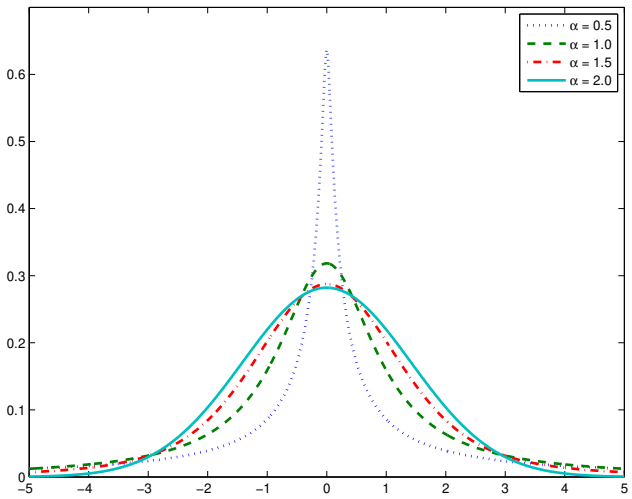

Figure 1: *Comparison of the PDFs of symmetric alpha-stable distributions with* $\alpha = 0.5$, $\alpha = 1$, $\alpha = 1.5$ *and* $\alpha = 2$. *The other parameters are set equal to* $\beta = 0$, $\gamma = 1$, $\delta = 0$.

values of α. The distribution with $\alpha = 2$ corresponds to the well known Gaussian distribution and the one with $\alpha = 1$ corresponds to the Cauchy distribution. Comparing the PDFs, we see that the tails of the bells become heavier as α decreases. In fact, the Cauchy bell ($\alpha = 1$) has thicker tail than the Gaussian distribution ($\alpha = 2$). Thus, the rare events have more probability of occurring in the Cauchy bell curve than in the Gaussian bell curve and for this reason, the noise generated from the Cauchy distribution is more impulsive than the Gaussian one. For instance, the Cauchy noise can contain powerful noise spikes that can be more than a hundred times the magnitude of the humbler Gaussian noise spikes.

In order to illustrate the difference between the Gaussian noise and the Cauchy noise, in Figure 2 we show a 1 Dimensional noise free signal and the corresponded degraded signal using the Gaussian noise and the Cauchy noise. The noisy signal corrupted by Gaussian noise has been obtained simply adding random values from the Gaussian distribution. From [40, 41], we know that the Cauchy noise can be obtained from the ratio of two independent Gaussian variables. Hence, to create the noisy signal with Cauchy noise, firstly we generate two vectors contained random values from the Gaussian distribution, and then we add the ratio between these two vectors to the original signal. From the figures, one can see that the Cauchy noise is much more impulsive than the Gaussian noise, thus the rare events have more probability to occur. Note that the vertical scale goes from 30 to 120 for the original signal and the one degraded by Gaussian noise, while it goes from -100 to 400 for the signal degraded by Cauchy noise.

Finally, we now describe how Cauchy noise influences the clean image. Given the original image $u : \Omega \to \mathbb{R}$, with $\Omega \subset \mathbb{R}^2$ be a bounded, open and connected set with compact Lipschitz boundary, the noisy image $f : \Omega \to \mathbb{R}$ is given by,

$$f = u + v,$$

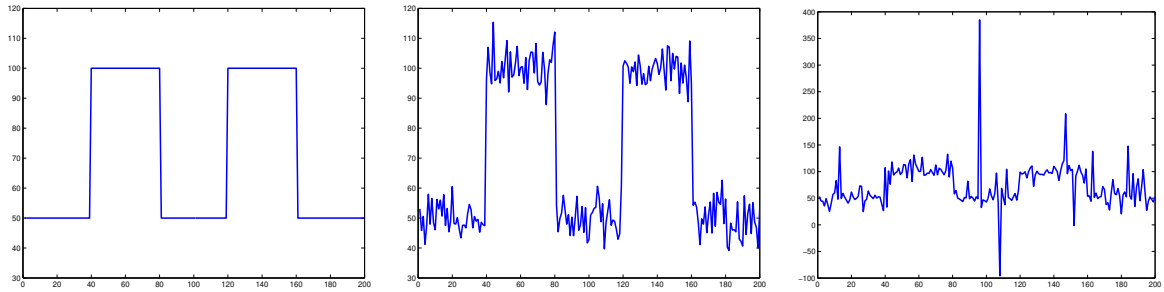

(a) Noise free signal. (b) Degraded by Gaussian noise. (c) Degraded by Cauchy noise.

Figure 2: *Symmetric alpha-stable noise in 1D: notice that the y-axis has different scale (scale between* 30 *and* 120 *on (a) and (b) and* -100 *and* 400 *on (c)). (a) 1D noise free signal; (b) signal degraded by an additive Gaussian noise (with mean 0 and variance 25); (c) signal degraded by an additive Cauchy noise* ($\gamma = 25$*). Cauchy noise is more impulsive than the Gaussian noise.*

where v represents the random noise that modeles a Cauchy distribution. A random variable V follows the Cauchy distribution, $V \sim \text{Cauchy}(\gamma, \delta)$, if it has density as in (1.1). Without loss of generality, from now on, in our analysis we consider $\delta = 0$.

3. Variational model.

In this section we analyse our variational model for deblurring and denoising images corrupted by Cauchy noise. In the first part, we focus only on the denoising case and using the Maximum a Posteriori (MAP) estimator (see [26]) we derive our nonconvex model. Then, we study some properties of our restoration model, i.e. the existence of a minimizer and the minimum maximum principle. Later, we incorporate a blurring operator K in our variational model for deblurring and denoising simultaneously an image corrupted by Cauchy noise and we show how a solution can be computed numerically.

3.1. Variational model via MAP estimator.

Our goal is to find a variation model to restore image corrupted by Cauchy noise, in particular, we want to recover the original image u, given the noisy image $f = u + v$, where v follows the Cauchy noise. Based on [3], we derive our model using the Bayes rule and the Maximum a Posteriori (MAP) estimator, see [26]. In the following, we denote the random variables with the capital letters F, U and V, the respective instances with the small letters f, u and v and the respective density functions with g_F, g_U and g_V.

As already said in the previous section, we assume that v follows a "zero-centered" Cauchy law, thus its density function is defined as follows,

$$g_V(v) = \frac{1}{\pi} \frac{\gamma}{\gamma^2 + v^2}.$$

Given the noisy image f, for restoring the original image U, we have to maximize the conditional probability $P(U|F)$. From Bayes's rule [26], we know

$$P(U|F) = \frac{P(F|U)P(U)}{P(F)}. \tag{3.1}$$

Based on (3.1), we can equivalently minimize

$$-\log(P(U|F)) = -\log(P(F|U)) - \log(P(U)) + \log(P(F)). \tag{3.2}$$

Since the quantity $P(F)$ is constant respect to the variable U, we just need to minimize $-\log(P(F|U)) - \log(P(U))$.

The pixels of our image are corrupted by Cauchy noise, thus for $x \in \Omega$, with Ω the set of the pixels of the image, we have

$$P(f(x)|u) = P_{u(x)}(f(x)) = \frac{\gamma}{\pi\big(\gamma^2 + (u(x) - f(x))^2\big)}.$$

Inspired from [3], we assume that U follows a Gibbs prior:

$$g_U(u) = \frac{1}{Z}\exp(-\beta J(u)),$$

where Z is the normalization factor, $\beta > 0$ and J is a non negative given function such as $J(u) = \int_\Omega |Du|$ (the notation will be explained in the next section).

Now, since the image is discretized and the pixels $x \in \Omega$ are mutually independent and identically distributed (i.i.d.), we have $P(U) = \prod_{x\in\Omega} P(U(x))$, where $U(x)$ is the instance of the random variable U at the pixels x. Hence, minimizing (3.2) is equivalent to minimize

$$-\log(P(F|U)) = -\sum_{x\in\Omega}\Big(\log\big(P(F(x)|U(x))\big) + \log\big(P(U(x))\big)\Big). \tag{3.3}$$

Substituting the explicit expressions of $\log P(F(x)|U(x))$ and $\log P(U(x))$ in (3.3), we can easily write (3.3) as follows,

$$-\log(P(F|U)) = \sum_{x\in\Omega}\Big(\log\big(\gamma^2 + (U(x) - F(x))^2\big) + \beta J(U(x)) + \log\pi + \log Z - \log\gamma\Big). \tag{3.4}$$

Since the last three terms are constants, our proposed functional for restoring images corrupted with Cauchy noise is given by

$$E(u) := \int_\Omega |Du| + \frac{\lambda}{2}\int_\Omega \log\Big(\gamma^2 + (u - f)^2\Big)\mathrm{d}x, \tag{3.5}$$

where λ is a strictly positive parameter.

In the following sections, we briefly recall the definition of the space of the functions bounded variation and we give some theoretical results about the existence of a minimizer.

3.2. Total variation regularization. In 1992, in order to restore corrupted images preserving edges in the image, total variation (TV) regularization was introduced by Rudin, Osher and Fatemi in [46]. In this work, they recover the image u in the space of the functions of bounded variation (BV). In particular, $u \in BV(\Omega)$ iff $u \in L^1(\Omega)$ and the seminorm in the space $BV(\Omega)$ is finite, where the BV-seminorm is defined as follows,

$$\int_\Omega |Du| := \sup\left\{\int_\Omega u\cdot \mathrm{div}(\xi(x))\mathrm{d}x \,\middle|\, \xi \in C_0^\infty(\Omega,\mathbb{R}^2), \|\xi\|_{L^\infty(\Omega,\mathbb{R}^2)} \le 1\right\}. \tag{3.6}$$

The space $BV(\Omega)$ endowed with the norm $\|u\|_{BV} = \|u\|_{L^1} + \int_\Omega |Du|$ is a Banach space. If $u \in BV(\Omega)$, (3.6) corresponds to the total variation. From the compactness of the space $BV(\Omega)$, we have the following embedding, $BV(\Omega) \hookrightarrow L^p(\Omega)$, with $1 \leq p \leq 2$, and for $p < 2$ it is compact (see [2] for more explanations).

3.3. Existence of a solution. Our proposed model to restore image corrupted by Cauchy noise is given by

$$\inf_{u \in BV(\Omega)} \int_\Omega |Du| + \frac{\lambda}{2} \int_\Omega \log\Big(\gamma^2 + (u-f)^2\Big) \mathrm{d}x, \tag{3.7}$$

where the $TV(u)$ is used as the regularization term, $\lambda > 0$ is the regularization parameter and $f \in L^\infty(\Omega)$ is the noisy image.

In the following theorem we prove that there exists at least one solution for our minimization problem (3.7).

Theorem 3.1. *Let f be in $L^\infty(\Omega)$, then the problem (3.7) has at least one solution in $BV(\Omega)$ satisfying:*

$$\inf_\Omega f \leq u \leq \sup_\Omega f.$$

Proof. Let's denote $a = \inf f$ and $b = \sup f$ and let's consider a minimizing sequence $\{u_n\} \in BV(\Omega)$ for (3.7). First of all, we show that we can assume $a \leq u_n \leq b$ without loss of generality and so the sequence $\{u_n\}$ is bounded in $L^1(\Omega)$. Fixing $x \in \Omega$ and denoting the data fidelity term with $h : \mathbb{R} \to \mathbb{R}$, where $h(t) := \log(\gamma^2 + (t - f(x))^2)$, we have

$$h'(t) = \frac{2\big(t - f(x)\big)}{\gamma^2 + \big(t - f(x)\big)^2}.$$

Thus, the function h is decreasing if $t < f(x)$ and increasing if $t > f(x)$. For every $M \geq f(x)$, we have

$$h(\min(t, M)) \leq h(t).$$

Hence, if $M = b$, we have

$$\int_\Omega \log\Big(\gamma^2 + \big(\inf(t,b) - f(x)\big)^2\Big) \mathrm{d}x \leq \int_\Omega \log\Big(\gamma^2 + \big(t - f(x)\big)^2\Big) \mathrm{d}x.$$

Furthermore, from [29], we know that $\int |D \inf(u,b)| \leq \int |Du|$. By definition of our functional E, we can conclude that $E(\inf(u,b)) \leq E(u)$. In the same way, we can prove that $E(\sup(u,a)) \leq E(u)$, with $a = \inf f$. Hence, since $a \leq u_n \leq b$, the sequence $\{u_n\}$ is bounded in $L^1(\Omega)$.

Now, applying our functional E to the sequence $\{u_n\}$, we have $E(u_n)$ is bounded. In particular, there exists a constant $C > 0$ such that $E(u_n) \leq C$. The data fidelity term has minimum value $2 \log \gamma$ when $u = f$ and $E(u_n)$ is bounded, hence also the regularization term $\int |D(u_n)|$ is bounded. Thus, the sequence $\{u_n\}$ is bounded in $BV(\Omega)$ and there exists $u \in BV(\Omega)$ such that up to a subsequence, we have $u_n \to u$ in $BV(\Omega)$-weak and $u_n \to u$ in $L^1(\Omega)$-strong. Furthermore, using $a \leq u \leq b$, the lower semi-continuity of the total variation and the Fatou's lemma, we have that u is a minimizer of the problem (3.7). ∎

Now, we are able to prove, under some hypothesis, that there exists a unique solution for our minimization problem (3.7).

Proposition 3.2. *Let f be in $L^\infty(\Omega)$, then the problem (3.7) has only one solution u such that $f-\gamma < u < f+\gamma$.*

Proof. Using the same notation as before and fixing $x \in \Omega$, we have

$$h''(t) = \frac{2\big(\gamma^2 - (t-f(x))^2\big)}{\big(\gamma^2 + (t-f(x))^2\big)^2},$$

where $t \in \mathbb{R}$. If $f-\gamma < t < f+\gamma$ the function h is strictly convex, hence there exists a unique minimizer for the problem defined in (3.7). ∎

In the following proposition we enunciate the minimum-maximum principle.

Proposition 3.3. *Let f_1 and f_2 be in $L^\infty(\Omega)$ with $a_1 = \inf_\Omega f_1$ and $a_2 = \inf_\Omega f_2$ and we denote $b_1 = \sup_\Omega f_1$ and $b_2 = \sup_\Omega f_2$. Let us assume that $f_1 < f_2$. Then, denoting with u_1 (resp. u_2) a solution of (3.7) for $f = f_1$ (resp. $f = f_2$), we have $u_1 \le u_2$, if $(b_2-a_1)(b_2-a_2) < 1$.*

Proof. From the Theorem (3.1), we know that the problem (3.7) admits solutions. Thus, by definition of u_1 and u_2 we have

$$J(u_1 \wedge u_2) + \frac{\lambda}{2}\int_\Omega \log(\gamma^2 + (u_1 \wedge u_2 - f_1)^2)\mathrm{d}x \ge J(u_1) + \frac{\lambda}{2}\int_\Omega \log(\gamma^2 + (u_1 - f_1)^2)\mathrm{d}x,$$

and

$$J(u_1 \vee u_2) + \frac{\lambda}{2}\int_\Omega \log(\gamma^2 + (u_1 \vee u_2 - f_2)^2)\mathrm{d}x \ge J(u_2) + \frac{\lambda}{2}\int_\Omega \log(\gamma^2 + (u_2 - f_2)^2)\mathrm{d}x,$$

where $u_1 \wedge u_2 = \inf(u_1, u_2)$ and $u_1 \vee u_2 = \sup(u_1, u_2)$. From [9, 22], we know $J(u_1 \wedge u_2) + J(u_1 \vee u_2) \le J(u_1) + J(u_2)$, thus, adding the two inequalities above we have,

$$\int_\Omega \Big(\log(\gamma^2+(u_1\wedge u_2-f_1)^2)-\log(\gamma^2+(u_1-f_1)^2)+\log(\gamma^2+(u_1\vee u_2-f_2)^2)-\log(\gamma^2+(u_2-f_2)^2)\Big)\mathrm{d}x \ge 0.$$

We now split the domain Ω into two parts $\Omega = \{u_1 > u_2\} \cup \{u_1 \le u_2\}$ and we deduce that

$$\int_{\{u_1>u_2\}} \Big(\log(\gamma^2+(u_2-f_1)^2)-\log(\gamma^2+(u_1-f_1)^2)+\log(\gamma^2+(u_1-f_2)^2)-\log(\gamma^2+(u_2-f_2)^2)\Big)\mathrm{d}x \ge 0.$$

Using the properties of the logarithm and collecting the terms $(f_1 - f_2)(u_1 - u_2)$, we can rewrite the above expression as follows,

$$\int_{\{u_1>u_2\}} (f_1-f_2)(u_1-u_2)\Big(2\gamma^2 + (f_1+f_2)(u_1+u_2) - 2(f_1f_2+u_1u_2)\Big)\mathrm{d}x \ge 0. \tag{3.8}$$

Hence, if the following inequality holds

$$2 + (f_1+f_2)(u_1+u_2) - 2(f_1f_2+u_1u_2) > 0, \tag{3.9}$$

we have the thesis of this proposition. In fact, since $f_1 < f_2$, we have that $\{u_1 > u_2\}$ has a zero Lesbegue measure, thus we have proved that $u_1 \leq u_2$ a.e. in the domain Ω.

Now, we prove that, under our hypothesis the inequality (3.9) holds. Introducing a new variable u in (3.9), such as $u^2 = u_1 u_2$, and using the Cauchy inequality, we can easily find that (3.9) is equivalent to the following inequality

$$(u - f_1)(u - f_2) < 1. \tag{3.10}$$

From the previous theorem, we know that $a_1 \leq u_1 \leq b_1$ and $a_2 \leq u_2 \leq b_2$, thus, by hypothesis that $f_1 < f_2$, we have $a_1 < u < b_2$. Hence, the inequality in (3.10) always holds if $(b_2 - a_1)(b_2 - a_2) < 1$. ■

3.4. Deblurring and denoising case. Since in the real applications the observed image f is not only corrupted by noise, but it is also blurred, we extend the minimization model in (3.7) to the deblurring and denoising case. In particular, the blurred and noisy image is given by $f = Ku + v$, where $K \in \mathcal{L}(L^2(\Omega))$ is a known linear and continuous blurring operator and $v \in L^2(\Omega)$, as above, represents the Cauchy noise. In the deblurring and denoising case, the minimization problem becomes

$$\inf_{u \in BV(\Omega)} \int_\Omega |Du| + \frac{\lambda}{2} \int_\Omega \log\Big(\gamma^2 + (Ku - f)^2\Big) \mathrm{d}x. \tag{3.11}$$

3.5. Steepest gradient descent. In this subsection, we show how to compute numerically a solution of (3.11). We consider directly the deblurring and denoising case, since (3.7) can be seen as a special case of (3.11), when K is the identity operator.

First of all, we derive the discrete version of our minimization problem (3.11) and then we study how to solve it numerically. For simplicity we keep the same notations from the continuous contest. Let $f \in \mathbb{R}^{mn}$ be the noisy image obtained from a two-dimensional pixel-array, with dimension $m \times n$, by concatenation in the usual columnwise fashion and $K \in \mathbb{R}^{mn \times mn}$ be the discretization of the continuous blurring operator K. The discrete version of our proposed minimization problem is given by

$$\min_u \|\nabla u\|_1 + \frac{\lambda}{2} \sum_i \log\Big(\gamma^2 + ((Ku)_i - f_i)^2\Big), \tag{3.12}$$

where the first term represents the discrete total variation of the image u and it is define as follows,

$$\|\nabla u\|_1 = \sum_i \sqrt{(\nabla_x u)_i^2 + (\nabla_y u)_i^2}.$$

The discrete gradient $\nabla \in \mathbb{R}^{2mn \times mn}$ is given by

$$\nabla u = \begin{pmatrix} \nabla_x u \\ \nabla_y u \end{pmatrix},$$

where the discrete derivative operators in the x-direction and y-direction, respectively, ∇_x and ∇_y, are obtained using the finite difference approximations to the derivatives with symmetric

boundary conditions,

$$(\nabla_x u)_{l,j} = \begin{cases} u_{l+1,j} - u_{l,j}, & \text{if } l < n \\ 0 & \text{if } l = n \end{cases} \quad \text{and} \quad (\nabla_y u)_{l,j} = \begin{cases} u_{l,j+1} - u_{l,j}, & \text{if } j < m \\ 0 & \text{if } j = m. \end{cases}$$

As [3], in order to solve the problem in (3.12), we use a steepest gradient descent approach, and we have

$$\frac{\partial u}{\partial t} = \operatorname{div}\left(\frac{\nabla u}{\|\nabla u\|_1}\right) + \lambda \frac{Ku - f}{\gamma^2 + (Ku - f)^2},$$

where the operations above are pointwise. Thus, for a small parameter $\delta_t > 0$, a solution of the minimization problem is given by

$$\frac{u_{t+1} - u_t}{\delta_t} = \operatorname{div}\left(\frac{\nabla u_t}{\sqrt{\|\nabla u_t\|_1^2 + \alpha^2}}\right) + \lambda K^\top \left(\frac{Ku_t - f}{\gamma^2 + (Ku_t - f)^2}\right), \tag{3.13}$$

where $\operatorname{div} = -\nabla^\top \in \mathbb{R}^{mn \times 2mn}$ is the divergence operator and $\alpha > 0$ is a small fixed parameter which ensures that the denominator is different from zero.

4. Convex variational model.

In this section we introduce a convex variation model for deblurring and denoising an image corrupted by Cauchy noise. At the beginning, we focus only on the denoising case and then we generalize the model for the deblurring case. Drawing inspiration from the nonconvex model defined in (3.7), we introduce a new model by adding a quadratic penalty term that is based on the image given by applying the median filter to the noisy image f. The reason why we choose to use the median filter will be explained in the paragraph 4.1.

In particular, introducing a quadratic penalty term into the previous nonconvex model (3.7), we have

$$\inf_{u \in BV(\Omega)} \int_\Omega |Du| + \frac{\lambda}{2}\left(\int_\Omega \log\left(\gamma^2 + (u - f)^2\right) \mathrm{d}x + \mu \|u - u_0\|_2^2\right), \tag{4.1}$$

where u_0 is the image obtained applying the median filter to the noisy image f and $\lambda > 0$ and $\mu > 0$ are the regularization parameters. In this way, we will prove that the model, under some assumptions, is strictly convex and we will not have anymore issues about the uniqueness of the solution and the convergence of our numerical algorithm.

4.1. Median filter.

In this part we explain the reason why we choose the median filter [20] as a quadratic penalty term, focusing on the analogies between the Cauchy noise and impulse noise. Due to its simplicity and its capability of preserving image edges, in the past decades, the median filter has attracted much attention in the image processing [7, 30, 35, 48], especially for denoising images corrupted by impulse noise, see [13, 17]. Given the original image u, the noisy image f corrupted by impulse noise is defined as follows,

$$f(x) = \begin{cases} u(x) & \text{with probability } 1 - \sigma \\ \eta & \text{with probability } \sigma, \end{cases} \quad \text{with } x \in \Omega,$$

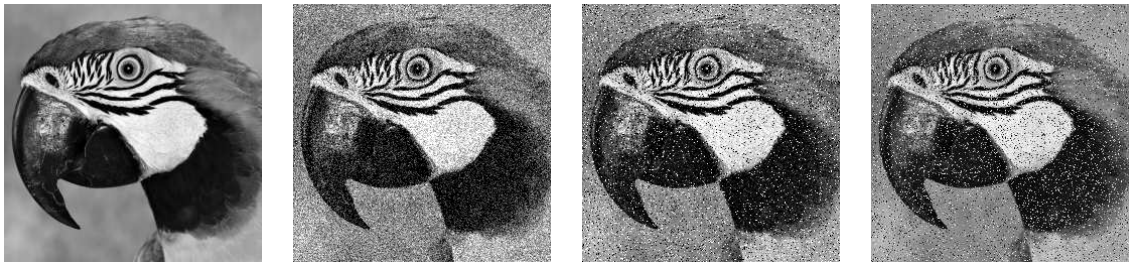

(a) Original image (b) Gaussian noise (c) Cauchy noise (d) Impulse noise

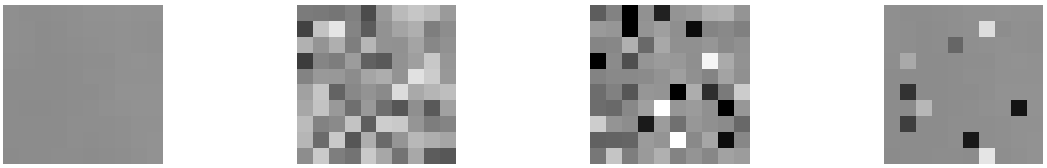

(e) Zoom of (a) (f) Zoom of (b) (g) Zoom of (c) (h) Zoom of (d)

Figure 3: *Comparison of different noisy images. (a) Original image* $u0$*; (b)* u *corrupted by an additive Gaussian noise (with mean 0 and variance 0.15); (c)* u *corrupted by an additive Cauchy noise (*$\gamma = 0.05$*); (d)* u *corrupted by an impulse noise (*$\sigma = 0.15$*); (e)–(h) zoom of the top left corner of the images (a)–(d), respectively. Cauchy noise and impulse noise are more impulsive than the Gaussian noise.*

where η is a uniformly distributed random variable with values in $[\min u, \max u]$ and $\sigma > 0$ is the noise level.

Figure 3(a) shows the original Parrot image and Figures 3(b), 3(c), and 3(d), respectively, represent the images corrupted by additive Gaussian noise, impulse noise and Cauchy noise. In Figures 3(e)–3(h) we show the zooms of the top left corner of 3(a)–3(d). One can see that the image degraded by Gaussian noise looks slightly different from the images corrupted by Cauchy noise and impulse noise, while in someway Cauchy noise and impulse noise are quite close each others. For instance, in the impulse noise and in the Cauchy noisy there are some pixels equal to white or black, while the image corrupted by Gaussian noise is uniformly modified and white and black pixels are very rare. Although Cauchy noise has some analogies with the impulse noise, there are also some very important differences, for instance in the impulse noise some pixels are noise free (see Figure 3(h)), while in the Cauchy noise all the pixels are corrupted by noise (see Figure 3(g)). Thus, due to the impulsive character of the Cauchy noise and to its analogies with the impulse noise, we decide to employ the median filter in our minimization problem (4.1).

In the literature, there exist also some filters created for removing noise in impulsive environments, for instance the myriad filter [24, 25]. The myriad filter theory is based on the definition of the sample myriad as the maximum likelihood location estimator of the alpha-stable distribution. It is a very robust filter for suppressing impulsive noise, in particular alpha-stable noise, but it is controlled by a parameter and the computational time is relativity long. For these reasons, we decided to employ the median filter instead of the myriad filter.

4.2. Existence and uniqueness of a solution. We now prove that the convex minimization problem defined in (4.1) is strictly convex and that the minimizer is unique

Proposition 4.1. *If $8\mu\gamma \geq 1$, the model defined in (4.1) is strictly convex.*

Proof. We start to prove that the data fidelity term in (4.1) is strictly convex. Fixed $x \in \Omega$ we define a function $h : \mathbb{R} \to \mathbb{R}$ as

$$h(t) := \log\Big(\gamma^2 + \big(u - f(x)\big)^2\Big)^2 + \mu\Big(t - u_0(x)\Big)^2 \tag{4.2}$$

and we prove that is strictly convex. Easily, we can compute the first and the second order derivative of h, and we have

$$h'(t) = 2\frac{t - f(x)}{\gamma^2 + (t - f(x))^2} + 2\mu(t - u_0(x)) \quad \text{and} \quad h''(t) = 2\frac{\gamma^2 - (t - f(x))^2}{\big(\gamma^2 + (t - f(x))^2\big)^2} + 2\mu.$$

A direct computation, show that h is strictly convex for $8\mu\gamma^2 \geq 1$. Since total variation regularization is convex, we can also conclude that the objective function in (4.1) is strictly convex, for $8\mu\gamma^2 \geq 1$, and hence we have the thesis. ∎

We now prove the existence and uniqueness of a solution to (4.1).

Theorem 4.2. *Let f be in $L^\infty(\Omega)$, then the model (4.1) has a unique solution $u \in BV(\Omega)$ satisfying*

$$\min\{\inf_\Omega f, \inf_\Omega u_0\} \leq u \leq \max\{\sup_\Omega f, \sup_\Omega u_0\}.$$

Proof. In order to prove the existence of a solution to (4.1) we can repeat the proof in Theorem 3.1. In fact, also in this case the function defined in (4.2) is decreasing if $t < \min\{\inf f, \inf u_0\}$ and it is increasing if $t > \max\{\sup f, \sup u_0\}$.

The uniqueness of the solution follows directly from the strict convexity of our model. ∎

As in section 3, we enunciate the minimum-maximum principle for the convex minimization problem. The proof of this proposition follows the same arguments as in the Proposition 3.3.

Proposition 4.3. *Let f_1 and f_2 be in $L^\infty(\Omega)$ with $a_1 = \inf_\Omega f_1$ and $a_2 = \inf_\Omega f_2$ and we denote $b_1 = \sup_\Omega f_1$ and $b_2 = \sup_\Omega f_2$. Let us assume that $f_1 < f_2$. Then, denoting with u_1 (resp. u_2) a solution of (4.1) for $f = f_1$ (resp. $f = f_2$), we have $u_1 \leq u_2$, if $(b_2 - a_1)(b_2 - a_2) < 1$.*

4.3. Deblurring and denoising case. We now modify our model to include a linear and continuous blurring operator $K \in \mathcal{L}(L^2(\Omega))$. To restore a blurred image corrupted by Cauchy noise, we introduce the following optimization problem,

$$\inf_{u \in BV(\Omega)} \int_\Omega |Du| + \frac{\lambda}{2}\left(\int_\Omega \log\Big(\gamma^2 + (Ku - f)^2\Big)\mathrm{d}x + \mu\|Ku - u_0\|_2^2\right), \tag{4.3}$$

where u_0 is the image obtained applying the median filter to the blurred and noisy image f.

Since the blurring operator K is nonnegative and it is linear, we can conclude that the model in (4.3) is strictly convex. One can prove that the results about the existence and uniqueness of the minimizer and the minimum-maximum principle hold also in this general case.

4.4. Numerical method. In this part we show how to compute numerically the minimizer of (4.3). We focus directly on the general case, since the denoising case can be seen as a special case of deblurring and denoising one. As in the paragraph 3.5, for sake of simplicity we keep the notation from the continuous contest. Due to the strict convexity of (3.11), there exists many algorithms to solve the proposed model, for instance the primal dual algorithm [10, 15], the alternating direction method with multipliers (ADMM) [6], the split-Bregman algorithm [23] and the Chambolle-Pock algorithm [11]. Since, under some hypothesis, the convergence of the Chambolle-Pock algorithm is guaranteed, see [11], we decide to employ it to solve our minimization problem (3.11).

In order to compute numerically the solution of our minimization problem, we introduce the discrete version of (4.3),

$$\min_u \|\nabla u\|_1 + \frac{\lambda}{2} G(Ku), \tag{4.4}$$

where $K \in \mathbb{R}^{mn\times mn}$ is the blurring matrix obtained from the discretization of the operator K and $G : \mathbb{R}^{mn} \to \mathbb{R}$ is defined as follows

$$G(u) := \sum_i \log\Big(\gamma^2 + (u_i - f_i)^2\Big) + \mu\|u - u_0\|_2^2.$$

As in [14], for using the primal dual algorithm, we introduce two new variables $v \in \mathbb{R}^{2mn}$ and $w \in \mathbb{R}^{mn}$ and, instead of consider the unconstrained problem, we look at the following constrained optimization problem,

$$\min_{u,v,w} \|v\|_1 + \frac{\lambda}{2} G(w), \text{ subject to } v = (v_x, v_y)^\top = \nabla u \text{ and } w = Ku. \tag{4.5}$$

To apply the Chambolle-Pock algorithm, we study the primal dual optimization problem,

$$\min_{u,v,w\in\mathbb{R}^{mn}} \max_{p,q\in Y} \|v\|_1 + \frac{\lambda}{2} G(w) + \langle v - \nabla u, p\rangle + \langle w - Ku, q\rangle, \tag{4.6}$$

where $p \in \mathbb{R}^{2mn}$ and $q \in \mathbb{R}^{mn}$ are the dual variables, and $Y = \{q \in \mathbb{R}^{2mn} : \|q\|_\infty \le 1\}$, with $\|q\|_\infty$ is the ℓ^∞-vector norm and it is defined as follows

$$\|q\|_\infty = \max_{i\in\{1,\dots,mn\}} \sqrt{q_i^2 + q_{i+mn}^2}.$$

Then the Chambolle-Pock algorithm for solving (4.6) is described in Algorithm 1.

The objective functions (4.7) – (4.9) are quadratics, thus the update of p, q and u is given by

$$\begin{aligned} p^{k+1} &= \sigma(\bar{v}^k - \nabla\bar{u}^k) + p^k, \\ q^{k+1} &= \sigma(\bar{w}^k - K\bar{u}^k) + q^k, \\ u^{k+1} &= u^k + \tau(K^\top q^{k+1} - \mathrm{div} p^{k+1}). \end{aligned} \tag{4.15}$$

Algorithm 1 Solving (4.6), by using the Chambolle-Pock algorithm

1: Fixed $\sigma > 0$ and $\tau > 0$. Initialize: $p^0 = 0$, $q^0 = 0$, $u^0 = \bar{u}^0 = f$, $v^0 = \bar{v}^0 = \nabla u^0$ and $w^0 = \bar{w}^0 = Ku^0$.

2: Calculate p^{k+1}, q^{k+1}, u^{k+1}, v^{k+1}, w^{k+1}, $\bar{u}^{k+1}$, $\bar{v}^{k+1}$ and $\bar{v}^{k+1}$using the following equations:

$$p^{k+1} = \arg\max_p \langle \bar{v}^k - \nabla \bar{u}^k, p\rangle - \frac{1}{2\sigma}\|p - p^k\|_2^2, \tag{4.7}$$

$$q^{k+1} = \arg\min_q \langle \bar{w}^k - K\bar{u}^k, q\rangle - \frac{1}{2\sigma}\|q - q^k\|_2^2, \tag{4.8}$$

$$u^{k+1} = \arg\min_u -\langle \nabla u, p^{k+1}\rangle - \langle Ku, q^{k+1}\rangle + \frac{1}{2\tau}\|u - u^k\|_2^2, \tag{4.9}$$

$$v^{k+1} = \arg\min_v \|v\|_1 + \langle v, p^{k+1}\rangle + \frac{1}{2\tau}\|v - v^k\|_2^2, \tag{4.10}$$

$$w^{k+1} = \arg\min_w \frac{\lambda}{2}G(w) + \langle w, q^{k+1}\rangle + \frac{1}{2\tau}\|w - w^k\|_2^2, \tag{4.11}$$

$$\bar{u}^{k+1} = 2u^{k+1} - u^k, \tag{4.12}$$

$$\bar{v}^{k+1} = 2v^{k+1} - v^k, \tag{4.13}$$

$$\bar{w}^{k+1} = 2w^{k+1} - w^k. \tag{4.14}$$

3: Stop or set $k := k + 1$ and go back to step 2.

The equation in (4.10) can be rewritten in the following way,

$$v^{k+1} = \arg\min_v \|v\|_1 + \frac{1}{2\tau}\|v - t^k\|_2^2,$$

where $t^k = v^k - \tau p^{k+1}$. Thus, the update of v is easily given by applying the soft shrinkage operator,

$$v_i^{k+1} = \frac{t_i^k}{|t_i^k|}\max\{|t_i^k| - \tau, 0\} \text{ and } v_{i+mn}^{k+1} = \frac{t_{i+mn}^k}{|t_i^k|}\max\{|t_i^k| - \tau, 0\}, \text{ for } i = 1, \ldots, mn,$$

with $|t_i^k| = \sqrt{(t_i^k)^2 + (t_{i+mn}^k)^2}$.

The optimality condition for (4.11) is given by

$$\lambda\frac{w - f}{\gamma^2 + (w - f)^2} + \mu\lambda(w - u_0) + q^{k+1} + \frac{1}{\tau}(w - w^k) = 0, \tag{4.16}$$

where, as usual, the division and the exponentiation have to be considered pointwise. Easily, one can see that (4.16) is equivalent to cubic equation. From Cardano's formula, we can find the explicitly expression for the solutions of a cubic equation, see the following proposition. For more details, we refer the reader to [32].

Proposition 4.4. *A generic cubic equation with real coefficients*

$$ax^3 + bx^2 + cx + d = 0, \text{ with } a \neq 0 \tag{4.17}$$

has at least one solution among the real numbers. Let

$$q = \frac{3ac - b^2}{9a^2} \quad \text{and} \quad r = \frac{9abc - 27a^2d - 2b^3}{54a^3},$$

if there exists a unique real solution of (4.17)*, the discriminant,* $\Delta = q^3 + r^2$*, has to be positive. Furthermore, if* $\Delta \geq 0$*, the only real root of* (4.17) *is given by*

$$x = \sqrt[3]{r + \sqrt{\Delta}} + \sqrt[3]{r - \sqrt{\Delta}} - \frac{b}{3a}. \tag{4.18}$$

Due to the strict convexity of our problem, we know that there exists a unique real solution for (4.16) and, from the above proposition, it can be computed explicitly using (4.18). Otherwise, since the objective function in (4.11) has the second derivative, one can also determine the solution in a efficient way using the the Newton method following with one projection step, in order to guarantee the nonnegativity of u, see [18, 29]. In our simulations, we decide to compute the explicit expression of unique real solution using Cardano's formula.

We remark that, if K is the identity operator, i.e. the degraded image f is not blurred but it is only corrupted by noise, there is no need to introduce the primal variable w and the dual variable q, and the algorithm can be simplified accordingly.

In the last part of this section, we study the existence of the solution and the convergence of the algorithm. First of all, we reformulate (4.6) in the following way

$$\min_x \max_y \; H(x) + \langle Ax, y \rangle, \tag{4.19}$$

with $H(x) = \|v\|_1 + \frac{\lambda}{2} G(w)$ and

$$A = \begin{pmatrix} -\nabla & I & 0 \\ -K & 0 & I \end{pmatrix}, \quad x = \begin{pmatrix} u \\ v \\ w \end{pmatrix}, \quad \bar{x} = \begin{pmatrix} \bar{u} \\ \bar{v} \\ \bar{w} \end{pmatrix}, \quad y = \begin{pmatrix} p \\ q \end{pmatrix}.$$

Proposition 4.5. *The saddle-point set of* (4.19) *is nonempty.*

For the proof, we refer the reader to Proposition 2 in [37].

The following proposition shows the convergence of the algorithm described in Algorithm 1.

Proposition 4.6. *The iterates* (x^k, y^k) *defined in Algorithm 1 converge to a saddle point of the primal dual problem defined in* (4.19) *if* $\sigma\tau\|A\|_2^2 < 1$*, where* $\|A\|_2$ *denotes the operator 2-norm of* A*.*

This proposition can be seen as a special case of the Theorem 1 proved by Chambolle and Pock in [11].

In order to use the inequality given in the above proposition, we need to give an estimate of $\|A\|_2$. Easily, using the property of the norm, one can find that

$$\|Ax\|_2 \leq \sqrt{\|\nabla\|_2^2 + \|K\|_2^2}\|u\|_2 + \left\| \begin{pmatrix} v \\ w \end{pmatrix} \right\|_2.$$

(a) (b) (c)

Figure 4: *Original images. (a) Peppers; (b) Parrot; (c) Cameraman .*

If $\|x\|_2 = 1$, by definition of x, we have that $\|u\|_2^2 + \left\|\binom{v}{w}\right\|_2^2 = 1$, therefore, from Cauchy inequality, we obtain

$$\|Ax\|_2 \leq \sqrt{\|\nabla\|_2^2 + \|K\|_2^2 + 1}.$$

Hence, we have $\|A\|_2 \leq \sqrt{\|\nabla\|_2^2 + \|K\|_2^2 + 1}$.

From [10], we know that $\|\nabla\|_2^2 \leq 8$ and from [37], we have that $\|K\|_2 \leq 1$, thus $\|A\|_2 \leq \sqrt{10}$. Therefore, in order to ensure the convergence of our algorithm we just need that $\sigma\tau < 0.1$. In our numerical simulations we set $\sigma = \tau = 0.3$, which ensures the convergence of the algorithm.

5. Numerical simulations. In this section, we report some numerical reconstructions obtained applying our proposed model to blurred images corrupted by Cauchy noise. First of all, we focus only on the denoising case and then we consider also the deblurring case. In order to show the potentiality of our method, we compare our reconstructions with other images obtained employing other well known methods, as ROF model [46], the median filter [20] and the L^1-TV model. The L^1-TV model was introduced by Nikolova in [38, 39] for restoring images corrupted by impulse noise, in particular, in this model, the total variation regularization is combined with an L^1 data fidelity term. Motivated by the impulsive character of the Cauchy noise, we decide to compare our reconstructions also with the L^1-TV model. For the ROF model and the L^1-TV model, we employ the primal dual algorithm proposed in [11] to solve the minimization problem.

For illustrations, we use the 256-by-256 gray level images Peppers, Parrot and Cameraman, the original images are presented in Figure 4. The quality of the restored images is compared quantitatively using the peak signal noise ratio (PSNR) value [5] and the measure of structural similarity (SSIM) [52]. The PSNR is a measure widely used in image quality assessment and it is defined as follows,

$$\text{PSNR} = 20 \log_{10} \frac{mn|\max u - \min u|}{\|u^\star - u\|_2},$$

where $u^\star$ and u are respectively the restored and the original image. It is a very useful tool, since it is able to measure quantitatively the quality of the reconstruct image compare to the original image. Recently, another measure has become very popular among the imaging community, the so called SSIM measure. This measure compares local patterns of pixel

intensities that have been normalized for luminance and contrast and it has been proved that is more consistent with human eye perception than PSNR [52].

In our simulations, the regularization parameters of the variational model are tuned empirically. As a stopping rule, we decide to stop our algorithm as soon as there are not big changes in the objective function, i.e.

$$\frac{E(u^k) - E(u^{k-1})}{E(u^k)} < \varepsilon,$$

where ε is a small parameter and E denotes the objective function of the proposed minimization problem. In our experiments, we set $\varepsilon = 5 \cdot 10^{-5}$. In addition, all the simulations reported here are run in MATLAB R2014a.

5.1. Image denoising. Even our method works for simultaneously deblurring and denoising, in this section we focus only on the denoising case. Our aim is to recover the original image u, knowing the corrupted image f. Since the ratio of two independent standard normal variables gives a standard Cauchy random variable, we can generate the noisy image f using the following equality,

$$f = u + v = u + \gamma \frac{\eta_1}{\eta_2},$$

where the random variable v follows the Cauchy distribution, $\gamma > 0$ is the scale parameter and η_1 and η_2 follow the Gaussian distribution with mean 0 and variance 1.

In the following, we compare our reconstructions with the ones obtained applying the ROF model, the median filter (MD) and the L^1-TV model. As you will see, in average with our method we can improve the PSNRs of the recovered images of 0.55 dB.

Table 1: *PSNR values and SSIM measures for noisy images and recovered images given by different methods ($\gamma = 0.02$). In the last line of the table, we compute the average of the values.*

	PSNR					**SSIM**				
	Noisy	**ROF**	**MD**	**L^1-TV**	**Ours**	**Noisy**	**ROF**	**MD**	**L^1-TV**	**Ours**
Peppers	19.15	25.03	29.64	30.34	**30.94**	0.3243	0.4820	0.6743	0.7163	**0.7168**
Parrot	19.13	23.88	27.05	28.02	**28.98**	0.3179	0.4083	0.5894	0.6571	**0.6641**
Cameraman	19.07	24.00	26.14	27.21	**27.91**	0.2743	0.2314	0.4115	0.4715	**0.4707**
Lena	19.06	24.58	28.94	29.84	**30.36**	0.3240	0.4022	0.6488	0.6950	**0.6880**
Baboon	19.17	21.16	21.38	24.24	**24.96**	0.5174	0.2115	0.4231	0.6980	**0.6950**
Goldhill	18.99	24.40	26.80	28.23	**28.80**	0.3744	0.3191	0.5875	0.6692	**0.6811**
Boat	19.03	24.21	27.27	28.70	**29.20**	0.3566	0.3474	0.6437	0.6908	**0.6931**
Mean	19.09	23.89	26.75	28.08	**28.74**	0.3556	0.3431	0.5683	0.6568	**0.6584**

In Figure 5 and 8, we show the results for denoising the corrupted images Peppers, Parrot and Cameraman for different noise levels, $\gamma = 0.02$ and $\gamma = 0.04$. The first column represents the noisy image, in the others we show respectively the reconstructions given by the ROF model, the median filter, L^1-TV model and our model. In order to make evident the differences

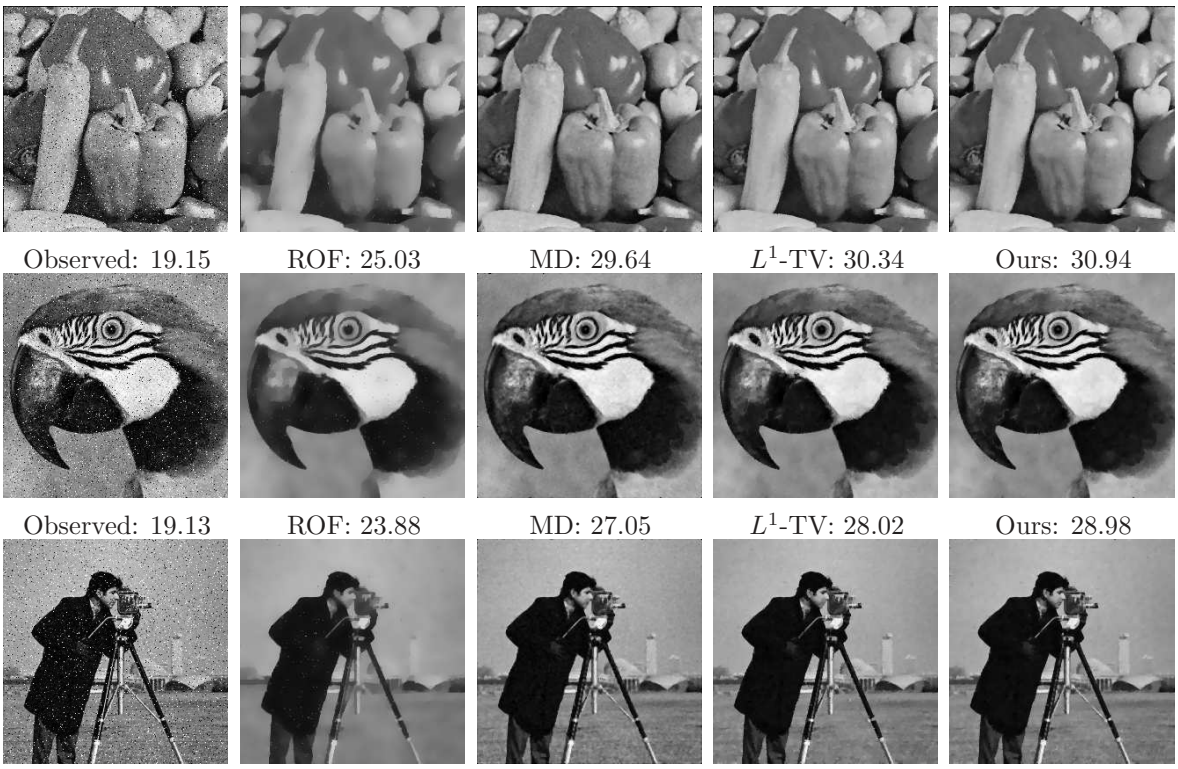

Figure 5: *Recovered images (with PSNR(dB)) of different approaches for removing Cauchy noise. First column: noisy images f ($\gamma = 0.02$); second column: restored images by ROF approach ($\lambda = 10$); third column: restored images by median filter (MD); forth column: restored images by L^1-TV approach ($\lambda = 1.5$); fifth column: restored images by our approach ($\lambda = 0.7$ and $\mu = 10$).*

between the reconstruction given by different approaches, in Figure 6, we present some details of Figure 5 (here, we also include the original image in the first column). The convergence of the algorithm of the three TV-based method is presented in Figure 7, where we plot the objective function values versus the number of iterations (we use the image of the Parrot when $\gamma = 0.02$). For the comparison of the performance quantitatively, in Table 1 and 2, we report the values of the PSNR and SSIM for the noisy and recovered images. In the tables, we also provide the values of PSNR and SSIM for other popular test images in image processing, i.e. Lena, Baboon, Goldhill, and Boat. Furthermore, after many simulations with different λ-values in the ROF model, the L^1-TV model and ours, we report the reconstructions that look visually better and give the best PSNRs.

Visually, it can be seen that L^1-TV model gives much better reconstructions than the ROF model and the median filter, and that our model reaches better visual quality and higher PSNR values. The reason why our method and the L^1-TV give good images, is because Cauchy noise is very impulsive and in some way it is very similar to impulse noise, see subsection 4.1. The ROF model was introduced for denoising image corrupted by Gaussian noise, in fact, it is not

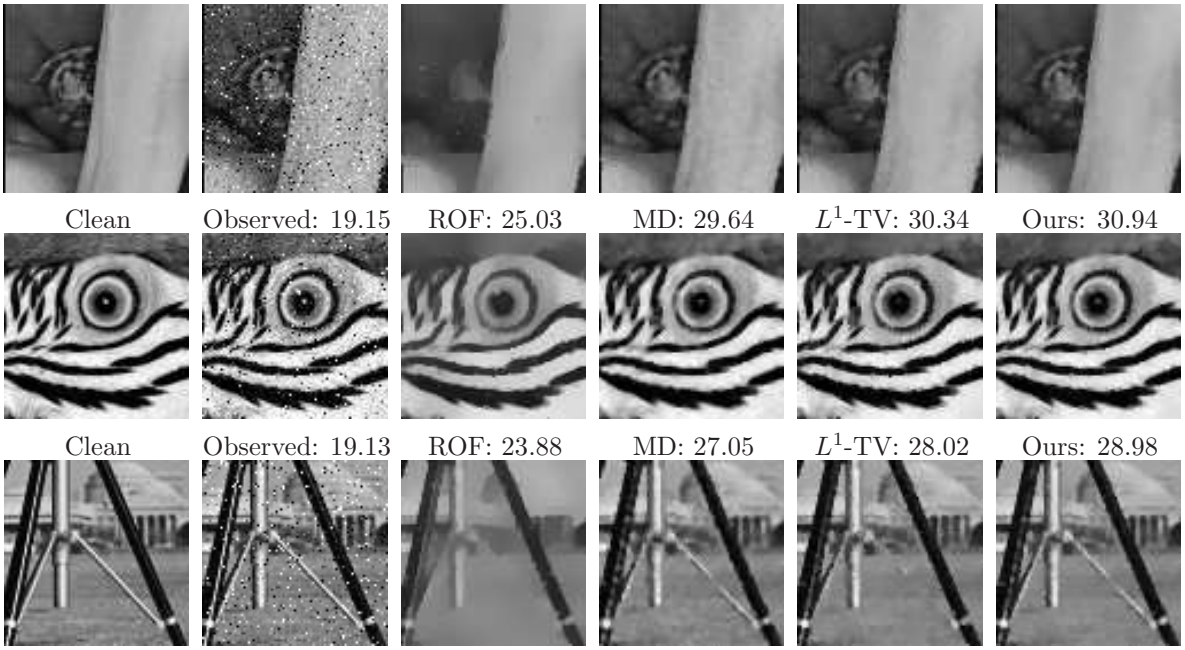

Figure 6: *The zoomed-in regions of the recovered images in Figure 5. First column: details of original images; second column: details of noisy images f ($\gamma = 0.02$); third column: details of restored images by ROF approach ($\lambda = 10$); forth column: details of restored images by median filter (MD); fifth column: details of restored images by L^1-TV approach ($\lambda = 1.5$); sixth column: details of restored images by our approach ($\lambda = 0.7$ and $\mu = 10$).*

able to denoise very well the degraded image with Cauchy noise, since it smooths too much the image, without preserving the details, especially in the cameraman we loose many details and it does not keep the contrast. The median filter works quite well if the noise level is low, otherwise it is not able to eliminate all the noise. From the details in Figure 6, we can see that our reconstructions preserve better the details of the image, i.e. the stalk of the peppers, the eye and the stripes of the parrot, the tripod and the column of the building in the cameraman. Considering also the respective tables, our method is able to improve in average the PSNR of 0.66 dB for $\gamma = 0.02$ and 0.55 dB for $\gamma = 0.04$ than the others methods.

5.2. Image deblurring and denoising. In this section, we consider blurred images corrupted by Cauchy noise. In our simulation, we test the Gaussian blur with a window size 9×9 and standard deviation of 1. After the blurring operation, we corrupt the images adding Cauchy noise with $\gamma = 0.02$. As in the previous section we compare our reconstructions with the ones obtained employing the ROF model, the median filter and the L^1-TV model, see Figure 9 and 10. In table 3, we report the values of the PSNR and SSIM for different images and different variational methods.

Comparing the results of the three TV-based methods, i.e. the ROF, the L^1-TV and our method, one can see that the proposed method performs best visually. In fact, the images

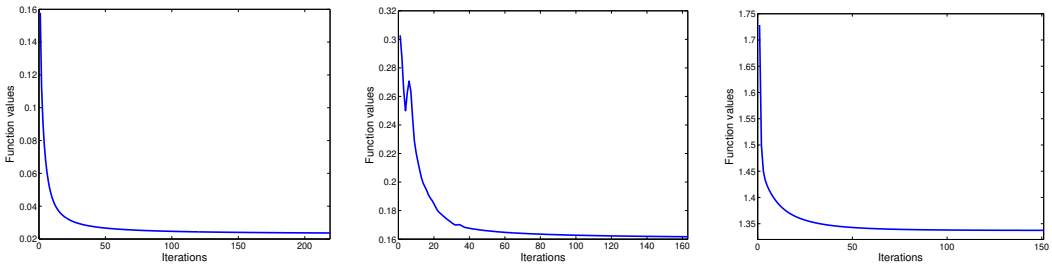

(a) (b) (c)

Figure 7: *Plots of the objective function values versus iterations of the three TV-based method corresponding to the experiments in the first line of Figure 5. (a) ROF model; (b) L^1-TV model; (c) our model.*

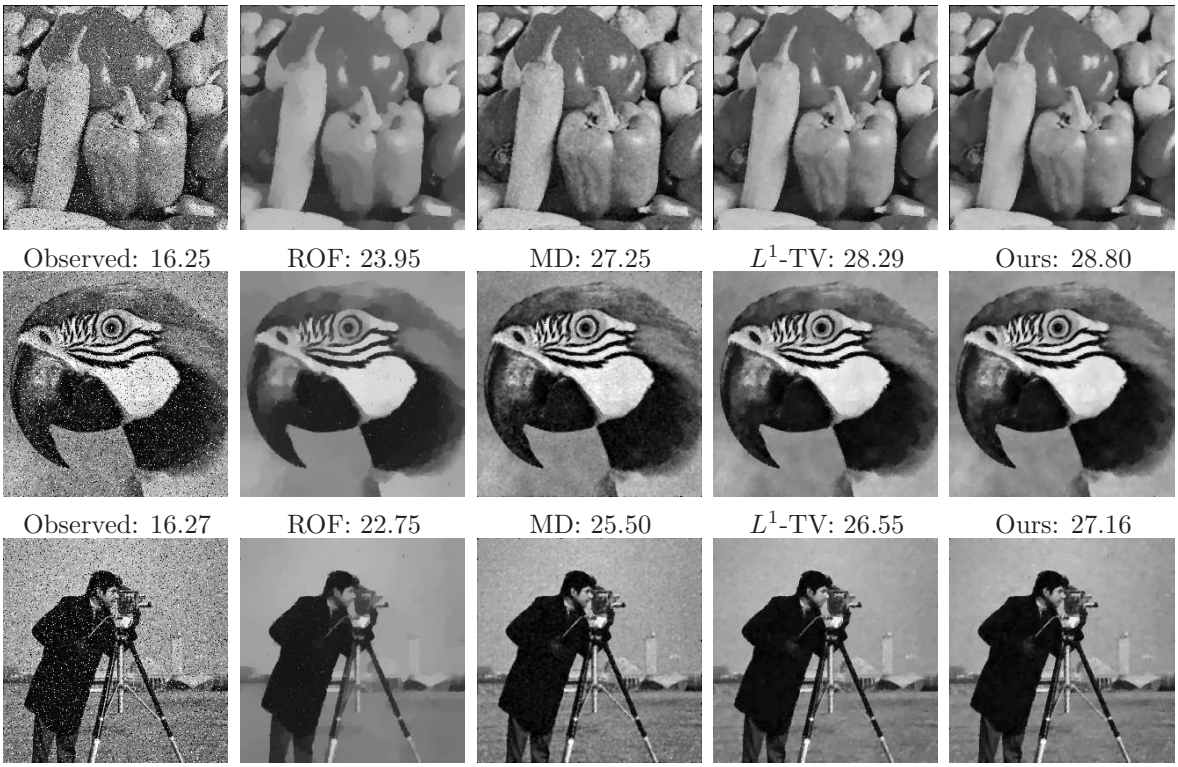

Observed: 16.25 ROF: 23.95 MD: 27.25 L^1-TV: 28.29 Ours: 28.80

Observed: 16.27 ROF: 22.75 MD: 25.50 L^1-TV: 26.55 Ours: 27.16

Observed: 16.08 ROF: 23.17 MD: 24.87 L^1-TV: 25.99 Ours: 26.66

Figure 8: *Recovered images (with PSNR(dB)) of different approaches for removing Cauchy noise. First column: noisy images f ($\gamma = 0.04$); second column: restored images by ROF approach ($\lambda = 9$); third column: restored images by median filter (MD); forth column: restored images by L^1-TV approach($\lambda = 1.3$); fifth column: restored images by our approach ($\lambda = 0.8$ and $\mu = 6$).*

Table 2: *PSNR values and SSIM measures for noisy images and recovered images given by different methods ($\gamma = 0.04$). In the last line of the table, we compute the average of the values.*

	PSNR					SSIM				
	Noisy	**ROF**	**MD**	**L^1-TV**	**Ours**	**Noisy**	**ROF**	**MD**	**L^1-TV**	**Ours**
Peppers	16.25	23.95	27.25	28.29	**28.80**	0.2246	0.4294	0.5605	0.6347	**0.6411**
Parrot	16.27	22.75	25.50	26.55	**27.16**	0.2334	0.3289	0.4706	0.5529	**0.5676**
Cameraman	16.08	23.17	24.87	25.99	**26.66**	0.1989	0.2081	0.3379	0.3857	**0.3920**
Lena	16.21	24.29	26.88	28.79	**29.30**	0.2220	0.4025	0.5394	0.5993	**0.6170**
Baboon	16.16	20.67	20.90	22.50	**23.05**	0.3651	0.1588	0.3681	0.5525	**0.5650**
Goldhill	16.21	23.72	25.48	26.49	**27.00**	0.2426	0.2786	0.5108	0.5205	**0.5684**
Boat	16.28	23.55	25.67	26.67	**27.18**	0.2479	0.3266	0.5429	0.5843	**0.5930**
Mean	16.21	23.16	25.22	26.47	**27.02**	0.2478	0.3047	0.4757	0.5471	**0.5634**

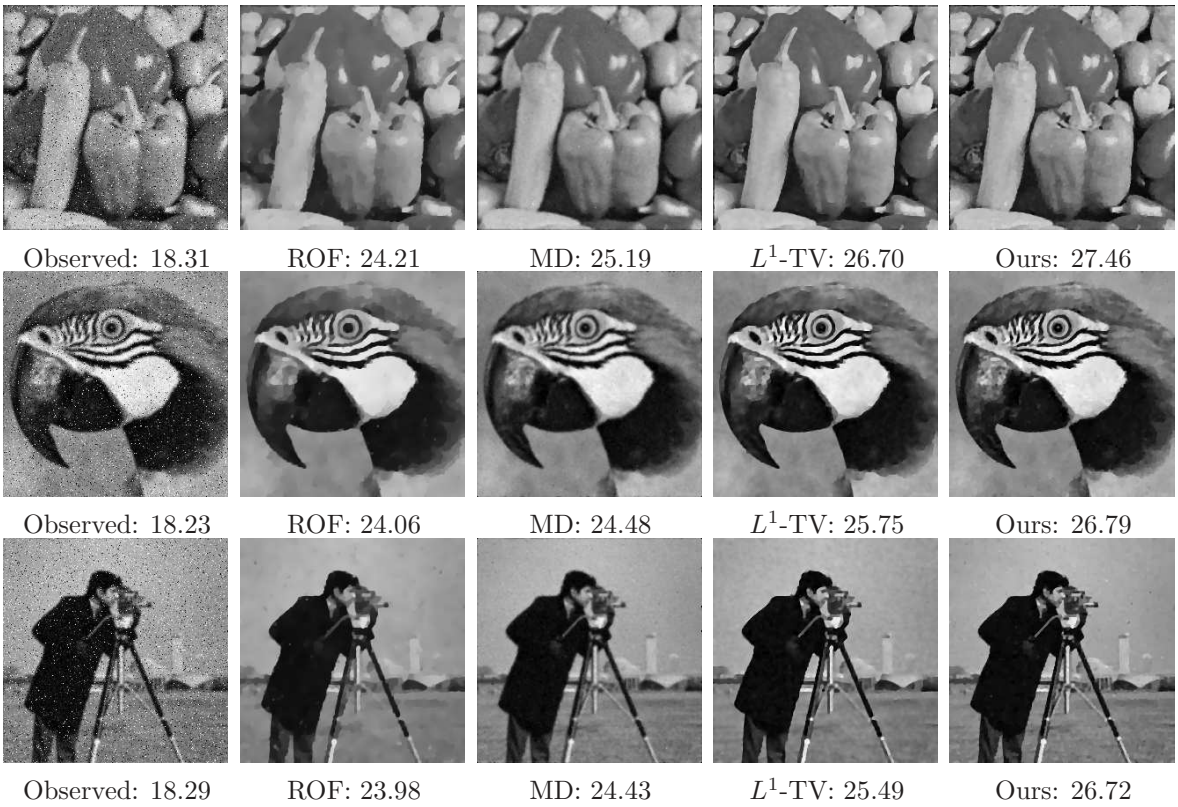

Figure 9: *Recovered images (with PSNR(dB)) of different approaches for deblurring and denoising of image blurred and corrupted by Cauchy noise. First column: blurred and noisy images f ($\gamma = 0.02$); second column: restored images by ROF approach ($\lambda = 14$); third column: restored images by median filter (MD); forth column: restored images by L^1-TV approach ($\lambda = 3$); fifth column: restored images by our approach ($\lambda = 2$ and $\mu = 30$).*

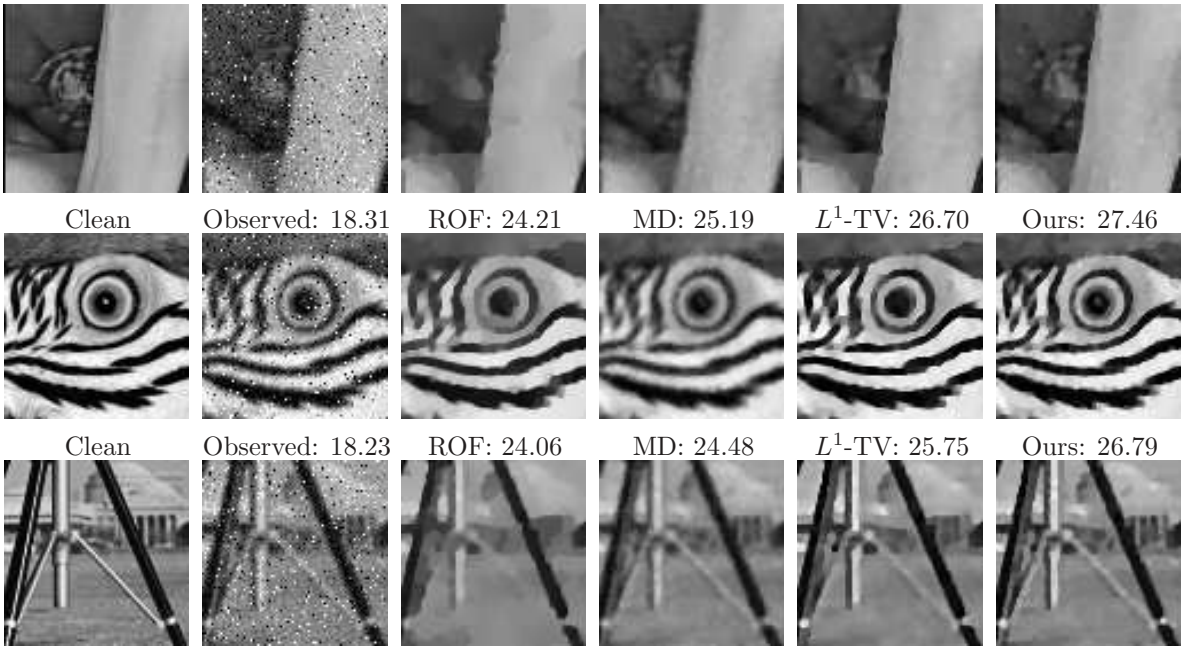

Figure 10: *The zoomed-in regions of the recovered images in Figure 9. First column: details of original images; second column: details of blurred and noisy images f ($\gamma = 0.02$); third column: details of restored images by ROF approach ($\lambda = 14$); forth column: details of restored images by median filter (MD); fifth column: details of restored images by L^1-TV approach ($\lambda = 3$); sixth column: details of restored images by our approach ($\lambda = 2$ and $\mu = 30$).*

given by the ROF model are too smooth and the details are missed (see, for instance, the detail of the peppers in Figure 10), L^1-TV preserves more details than the ROF model, but still some features are lost or not well recovered as in our model, such as the eye of the parrot and the columns of the building in the cameramen, see Figure 10. In the third column of Figure 9, the reconstructions given by the median filter are reported. One can note that the images are still blurred, this is because we do not employ any deblurred method but we just denoise the image using the filter. Visually and from the values of the PSNR and SSIM, we can clearly see that our method outperforms the others even in presence of blur.

6. Conclusion. In this paper, we introduce a variational method for deblurring and denoising of blurred images corrupted by Cauchy noise. In particular, inspired by the ROF model we combine a total variation regularization term with a data fidelity term suitable for the Cauchy noise. In order to obtain a convex minimization problem, we add a quadratic penalty term based on the median filter. Due to the strict convexity of our problem, we prove the existence and the uniqueness of a solution to our proposed model. Then, applying the primal dual algorithm, we solved our convex minimization problem and the convergence is ensured. The restored images show the efficiency and the capability of the proposed model comparing to other well known models, such as the ROF model, the median filter and the L^1-TV model.

Table 3: *PSNR values and SSIM measures for noisy images and recovered images given by different methods ($\gamma = 0.02$). In the last line of the table, we compute the average of the values.*

	PSNR					SSIM				
	Noisy	**ROF**	**MD**	**L^1-TV**	**Ours**	**Noisy**	**ROF**	**MD**	**L^1-TV**	**Ours**
Peppers	18.31	24.21	25.19	26.70	**27.46**	0.2413	0.4974	0.5909	0.6086	**0.6297**
Parrot	18.23	24.06	24.48	25.75	**26.79**	0.2316	0.4439	0.5145	0.5278	**0.5655**
Cameraman	18.29	23.98	24.43	25.49	**26.27**	0.1753	0.2609	0.3433	0.3516	**0.3880**
Lena	18.64	25.74	26.70	27.26	**28.14**	0.2487	0.4748	0.5764	0.5712	**0.6071**
Baboon	17.42	20.84	21.54	21.36	**21.81**	0.1955	0.2167	0.3573	0.3208	**0.3905**
Goldhill	18.47	24.84	25.88	26.17	**26.76**	0.2262	0.3678	0.5070	0.4911	**0.5390**
Boat	18.48	24.36	25.42	26.18	**26.69**	0.2410	0.4059	0.5313	0.5478	**0.5721**
Mean	18.28	24.00	24.81	25.56	**26.31**	0.2228	0.3811	0.4887	0.4884	**0.5274**

REFERENCES

[1] A. Achim and E. Kuruoğlu, *Image denoising using bivariate K-stable distributions in the complex wavelet domain*, IEEE Signal Process. Lett., 12 (2005), pp. 17-20.

[2] L. Ambrosio, N. Fusco, and D. Pallara, *Functions of Bounded Variation and Free Discontinuity Problem*, Oxford University Press, London, 2000.

[3] G. Aubert and J. Aujol, *A variational approach to removing multiplicative noise*, SIAM J. Appl. Math., 68 (2008), pp. 925–946.

[4] G. Aubert and P. Kornprobst, *Mathematical Problems in Image Processing. Partial Differential Equations and the Calculus of Variations*, Appl. Math. Sci. 147, Springer, New York, 2006.

[5] A. Bovik, *Handbook of Image and Video Processing*, Academic Press, New York, 2000.

[6] S. Boyd, N. Parikh, E. Chu, B. Peleato, and J. Eckstein, *Distributed optimization and statistical learning via the alternating direction method of multipliers*, Found. and Trends Mach. Learning, 3 (2010), pp. 1–122.

[7] D. Brownrigg, *The weighted median filter*, Commun. Ass. Comput. Mach., 27 (1984), pp. 807-818.

[8] J. Cai, R. Chan, and Z. Shen, *A framelet-based image inpainting algorithm*, Appl. Comput. Harmon. Anal., 24 (2008), pp. 131-149.

[9] A. Chambolle, *An algorithm for mean curvature motion*, Interface Free Bound., 4 (2004), pp. 1–24.

[10] A. Chambolle, *An algorithm for total variation minimization and applications*, J. Math. Imaging Vis., 20 (2004), pp. 89–97.

[11] A. Chambolle and T. Pock, *A first-order primal-dual algorithm for convex problems with applications to imaging*, J. Math. Imaging Vis., 40 (2011), pp. 120–145.

[12] Y. Chang, S. Kadaba, P. Doerschuk, and S. Gelfand *Image restoration using recursive markov random field models driven by cauchy distributed noise*, IEEE Signal Proc. Lett., 8 (2001), pp. 65–66.

[13] R. Chan, Y. Dong, and M. Hintermüller *An efficient two-phase L1-TV method for restoring blurred images with impulse noise*, IEEE Trans. Image Process., 19 (2010), pp. 1731–1739.

[14] R. Chan, H. Yang, and T. Zeng, *A two stage image segmentation method for blurry images with Poisson or multiplicative gamma noise*, SIAM J. Imaging Sci., 7 (2014), pp. 98–127.

[15] T. Chan, G. Golub, and P. Mulet, *A non-linear primal-dual method for total variation-based image restoration*, SIAM J. Sci. Comput. , 20 (1999), pp. 1964–1977.

[16] Y. Dong, M. Hintermüller, and M. Neri, *An efficient primal-dual method for L1 TV image restoration*, SIAM J. Imaging Sci., 2 (2009), pp. 1168–1189.

[17] Y. Dong and S. Xu, *A new directional weighted median filter for removal of random-valued impulse noise*, IEEE Signal Proc. Lett., 14 (2007), pp. 193–196.

[18] Y. Dong and T. Zeng, *A convex variational model for restoring blurred images with multiplicative noise*, SIAM J. Imaging Sci., 6 (2013), pp. 1598–1625.
[19] M. Elad and M. Aharon *Image denoising via sparse and redundant representations over learned dictionaries*, IEEE Tran. Image Process., 15 (2006), pp. 3736–3745.
[20] B. Frieden *A new restoring algorithm for the preferential enhancement of edge gradients*, J. Opt. Soc. Amer., 66 (1976), pp. 116–123.
[21] G. Gilboa and S. Osher *Nonlocal operators with applications to image processing*, Multiscale Model. Simul., 7 (2009), pp. 1005–1028.
[22] E. Giusti, *Minimal Surfaces and Funtions of Bounded Variation*, Birhäuser Boston, Cambridge, MA, 1984.
[23] T. Goldstein and S. Osher, *The split Bregman algorithm for L1-regularized problems*, SIAM J. Imaging Sci., 2 (2009), pp. 323–343.
[24] J. Gonzalez and G. Arce, *Optimality of the myriad filter in practical impulsive noise environments*, IEEE Trans. Signal Process., 49 (2001), pp. 438441.
[25] J. Gonzalez and G. Arce, *Weighted myriad filters: a robust filtering framework derived from alpha-table distributions*, IEEE Int. Conf. on Acoustics, Speech and Signal Process., 5 (1996).
[26] G. Grimmett and D. Welsh, *Probability: an Introduction*, Oxford Science Pubblications, London, 1986.
[27] M. El Hassouni and H. Cherifi, *Alpha-Stable Noise Reduction in Video Sequences*, ICIAR 1, A. C. Campilho and M. S. Kamel, eds., Springer, 2004, pp. 580–587.
[28] Y. Huang, L. Moisan, M. Ng, and T. Zeng, *Multiplicative noise removal via a learned dictionary*, IEEE Trans. Image Process, 21 (2012), pp. 4534–4543.
[29] Y. Huang, M. Ng, and Y. Wen, *A new total variation method for multiplicative noise removal*, SIAM J. Imaging Sci., 2 (2009), pp. 20–40.
[30] H. Hwang and R. Haddad, *Adaptive median filters: new algorithms and results*, IEEE Trans. Image Process., 4 (1995), pp. 499-502.
[31] M. Idan and J. Speyer, *Cauchy estimation for linear scalar systems*, IEEE Trans. Automatic Control, 55 (2010), pp. 1329–1342.
[32] N. Jacobson, *Basic Algebra*, Freeman, New York, 1974.
[33] B. Kosko, *Noise*, Viking Adult, 2006.
[34] E. Kuruoglu, W. Fitzgerald, and P. Rayner, *Near optimal detection of signals in impulsive noise modeled with asymmetric alpha-stable distribution*, IEEE Commun. Lett., 2 (1998), pp. 282–284.
[35] H. Lin and A. N. Willson, *Median filter with adaptive length*, IEEE Trans. Circuits Syst., 35 (1988), pp. 675-690.
[36] T. Le, T. Chartrand, and T. Asaki, *A variational approach to reconstructiong images corrupted by Poisson noise*, J.Math. Imaging Vis., 27 (2007), pp. 257–263.
[37] L. Ma, M. Ng, J. Yu, and T. Zeng, *Efficient box-constrained TV-type-l^1 algorithms for restoring images with impulse noise*, J. Comput. Math., 31 (2013), pp. 249–270.
[38] M. Nikolova, *Minimizers of cost functions involving nonsmooth data fidelity terms. Application to the processing of outliers*, SIAM J. Numer. Anal., 40 (2002), pp. 965–994.
[39] M. Nikolova, *A variational approach to remove outliers and impulse noise*, J. Math. Imaging Vis., 20 (2004), pp. 90–120.
[40] J. Nolan, *Numerical calculation of stable densities and distribution functions*, Comm. Statist. Stochastics Models, 13 (1997), pp. 759–774.
[41] J. Nolan, *Stable Distributions - Models for Heavy Tailed Data*, Birkhäuser Boston, 2015 (in progress: Chapter 1 online at academic2.american.edu/∼jpnolan).
[42] T. Pander, *New ploynomial approach to myriad filter computation*, Signal Process., 90 (2010), pp. 1991–2001.
[43] Y. Peng, J. Chen, X. Xu, and F. Pu, *SAR images statistical modeling and classification based on the mixture of alpha-stable distributions*, Remote Sens., 5 (2013), pp. 2145–2163.
[44] P. Reeves, *A non-Gaussian turbulence simulation air force flight dynamics laboratory*, Tech. Rep. AFFDL-TR-69-67, 1969.
[45] L. Rudin, P. Lions, and S. Osher, *Multiplicative denoising and deblurring: theory and algorithms*, S. Osher and N. Paragios, eds, Geometric Level Sets in Imaging, Vision and Graphics, pp. 103–119, Springer, 2003.

[46] L. Rudin, S. Osher, and E. Fatemi, *Nonlinear total variation based noise removal algorithms*, Phys. D, 60 (1992), pp. 259–268.
[47] G. Samorodnitsky and M. Taqqu, *Stable Non-Gaussian Random Processes: Stochastic Models with Infinite Variance*, Chapman & Hall, New York, 1994.
[48] T. Sun and Y. Neuvo, *Detail-preserving median based filters in image processing*, Pattern Recognition Lett., 15 (1994), pp. 341-347.
[49] T. Wan, N. Canagarajah, and A. Achim, *Segmentation of noisy colour images using cauchy distribution in the complex wavelet domain*, IET Image Process., 5 (2011), pp. 159–170.
[50] C. Wu and X. Tai, *Augmented Lagrangian method, dual methods, and split Bregman iteration for ROF, vectorial TV, and high order models*, SIAM J. Imaging Sci., 3 (2010), pp. 300-339.
[51] Y. Xiao, T. Zeng, J. Yu, and M. Ng, *Restoration of images corrupted by mixed Gaussian-impulse noise via $\ell_1 - \ell_0$ minimization*, Pattern Recognition, 44 (2011), pp. 1708–1728.
[52] W. Zhou, A. Bovik, H. Sheikh, and E. Simoncelli *Image Qualifty Assessment: From Error Visibility to Structural Similarity*, IEEE Trans. Image Process., 13 (2004), pp. 600-612.